International Journal of Fracture (2005) 132:153–173
DOI 10.1007/s10704-005-0671-x

Identification of embedded interlaminar flaw using inverse analysis

NARAYANAN RAMANUJAM[1], TOSHIO NAKAMURA[1,*] and MASATAKA URAGO[2]
[1]*Department of Mechanical Engineering, State University of New York at Stony Brook, Stony Brook, NY 11794*
[2]*Department of International Development Engineering, Tokyo Institute of Technology, Tokyo 152-8550, Japan*
**Author for correspondence (E-mail: toshio.nakamura@sunysb.edu)*

Received 24 June, 2004; accepted in revised form 13 January 2005

Abstract. The integrity of a composite laminate can be greatly affected by an existence of embedded interlaminar flaw. In general, identification of such a flaw often requires expensive tools and tedious processes. The aim of the present work is to develop a novel method with the aid of an intelligent post-processing scheme, thereby not relying on those sophisticated experiments. Essentially the proposed procedure utilizes an inverse analysis to estimate unknown delamination parameters from limited measurements. The procedure first constructs approximate functions relating the delamination parameters to measurement parameters. Then, a multi-dimensional minimization technique is adopted to search for the best estimates of unknown parameters corresponding to the lowest value of error objective function. In the present verification and simulation analyses, surface strains at discrete locations on a composite laminate under three-point bending are selected as the input measurements. Although reasonable estimates are obtained with these measurements, to increase their accuracy, the deflection at load point is also included as measurement input. Additional improvements are observed when those measurements under multiple loading conditions are included. A detailed error sensitivity analysis is also carried out to confirm the method's robustness. These results suggest the current method to be one of the alternate identification approaches for detecting a single embedded delamination in composite laminates.

Key words: Composite laminate, downhill simplex method, genetic algorithm, interlaminar flaw, inverse analysis.

1. Introduction

Composite laminates such as carbon fiber reinforced plastics (CFRP) are widely used in various engineering applications including aerospace, mechanical, and civil engineering owing to their excellent mechanical properties. However, their properties may significantly weaken when embedded interlaminar flaws/delaminations are introduced due to mal-fabrication process, imperfections, misalignment of fibers, and cyclic loads. Due to the mismatch in material properties of lamina, cross-plies are prone to decohesion between lamina. Figure 1 shows the micrograph of $[0/90]_{2s}$ cross-ply containing an embedded delamination. The delamination was generated during 100,000 tensile load cycles at 50% of ultimate load. The weakening of interlaminar bonding can also take place when composites are subjected to harsh environmental conditions of high temperature and humidity.

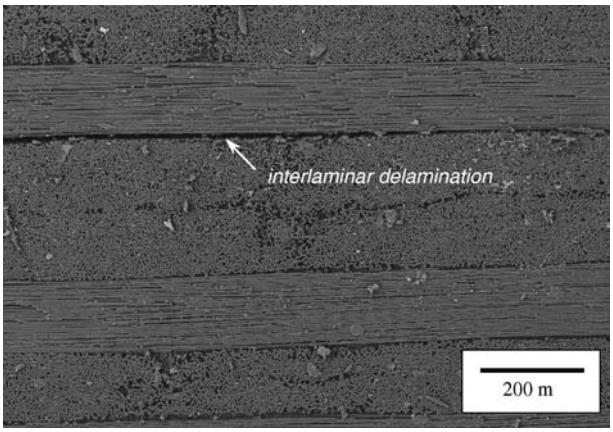

Figure 1. SEM micrograph showing interlaminar delamination of $[0/90]_{2s}$ cross-ply. The composite laminate was subjected to 100,000 fatigue cycles of uniaxial load at 50% of ultimate tensile load.

Composite laminates with delamination may no longer retain designed strength when subjected to large impact or compressive loads. In fact, they can fail by various failure modes such as global and local buckling, kink band formation and broadening and/or delamination growth as characterized by Wu et al. (1998) where various failure modes were identified for flat panels and cylindrical shells. Nakamura et al. (1995) also showed that embedded delamination in composite could trigger a collapse at lower loads than the original critical buckling load. The delamination behaviors under dynamic loadings were studied by Grady and Sun (1986), Sun and Manoharan (1989) and Wang et al. (1984). These investigations underlined the importance of identifying such a delamination to assess the residual strength of a composite panel and prevent possible catastrophic failures. However, embedded flaw detection in composites is usually more difficult and complex than in homogenous plates due to their complex structural arrangement.

Commonly, non-destructive evaluation (NDE) techniques such as ultrasonic inspection, electric resistance method, vibration response, infrared thermal images, and eddy current test are used to detect delamination type defects. Sakagami and Ogura (1994) employed infrared thermal images to detect the delamination with singular and insulation methods. Aymerich and Meili (2000) performed an ultrasonic inspection to detect delamination and discussed the combination of normal and oblique incidence pulse-echo ultrasonic techniques. Leung et al. (2001) introduced the fiber-optic interferometric technique where integrated strain along an embedded or surface attached fiber was measured as a function of load position. The eddy current test to detect delamination with special probes was shown by Mook et al. (2001). Xu et al. (2001) adopted a neural network to obtain estimates of delamination location and length from time-harmonic response of the specimen. Todoroki (2001) performed the electric resistance method to detect delamination in CFRP laminates and determined the required number of electrodes with the neural network and response surface method. Recently, piezoelectric materials have been used to detect delamination type defects. For an example, Tan and Tong (2004) have developed a one-dimensional analytical model to detect an embedded delamination using a piezoelectric fiber reinforced composite sensor and actuator. Yan and Yam (2004) detected tiny and

local delamination in composite laminates using piezoelectric patches by studying dynamic responses of structure. Regardless of the method, most of these investigations require complex/expensive tools to detect flaws and damages. A recent review of NDE techniques by McCann and Forde (2001) also noted the high cost of inspection.

The main goal of this study is to explore an alternate detection method that does not rely on expensive measurement tools but still offers robust delamination identification. An efficient inverse method that post-processes the limited measured record is proposed. Recently, inverse analysis approaches are being increasingly implemented in mechanical problems. For an example, Frederiksen (1997) has proposed an inverse approach for the identification of elastic properties of orthotropic plates. Moreover, various inverse analysis based techniques have been applied to detect delamination type flaws. Liu and Chen (2001) have used an inverse technique to identify the presence, location and orientation of flaw in the core layer of sandwiched plates. Here, the response of plates was initially estimated by finite element analysis. A genetic algorithm was also employed to search the flaw parameters. Ishak et al. (2001) have shown an adaptive multi-layer perceptron (MLP) network for inverse identification of interfacial delaminations in carbon/epoxy laminated composite beams.

When complex materials such as composites are inspected, it is essential to have an *intelligent* process to filter out critical information from available measurement. The proposed inverse method is designed to process those measurements that do not relate directly to the unknown parameters. Here the unknown delamination parameters are the location and size of the embedded flaw while the indirect measurements were chosen as surface strains and load-point deflections. The details of the procedure and the manner of implementation are described next.

2. Inverse analysis approach

The physical responses of many complex systems can be defined by a set of model/state parameters that are not directly measurable. It is however possible to define observable/measurable parameters that have relations with unknown state parameters (Tarantola, 1987). In this study, unknown parameters were set as the location and size of interlaminar delamination, and strain and deflection measurements are selected as the observable/measurable data.

In the approach to determine these unknowns, an inverse analysis is utilized here. Often, in this type of work, a major effort is consumed in finding an appropriate inverse procedure for the intended purpose. An improper method can lead to erroneous estimation. Furthermore, once the suitable technique is chosen, it must be tailored to fit the given problem. These processes take intensive trials and error study. In the current method, an objective function, which quantifies an accuracy of estimates, is first formulated. Here, forward/reference solutions that relate measured parameters to the unknown parameters are also established. Then an inverse process was required to find the unknown parameters that yield the lowest value of error objective function. These values are regarded as the best estimates of unknowns. In this analysis, the search for the best estimates is carried out with the *downhill simplex method,* which is a multi-dimensional minimization algorithm. The details of this algorithm are described in Section 2.4.

2.1. Embedded delamination model

To verify the procedure, a four-ply $[0/90]_s$ composite laminate containing the embedded flaw as shown in Figure 2a is considered. Here, the delamination location is measured from the mid-span to the center of delamination and denoted as s. Also the delamination length is denoted as $2a$. The through-thickness interlaminar delamination is assumed to be embedded between the 3rd and 4th layers from the top. Although this depth location of delamination is pre-determined, our separate analysis showed the delamination depth location to have a small effect in estimating the unknown parameters, s and $2a$, respectively. Furthermore, the present model can be easily modified for cross-ply composite laminates with many more layers. In such laminates, the exact depth location of delamination cannot be determined. However, in general, the ply-interface locations of delaminations are not so critical in assessing the residual strength of composite laminate. If the laminate were to be repaired, the entire section must be fixed. Similarly, if *multiple* delaminations exist near the same in-plane location but at different ply-interfaces, the present method should still be able to estimate the (in-plane) delamination location albeit with a slightly longer delamination estimate. In other words, the criticality due to existence of delaminations in such cases can be approximated with the present method with single delamination assumption. However, when multiple delaminations are not

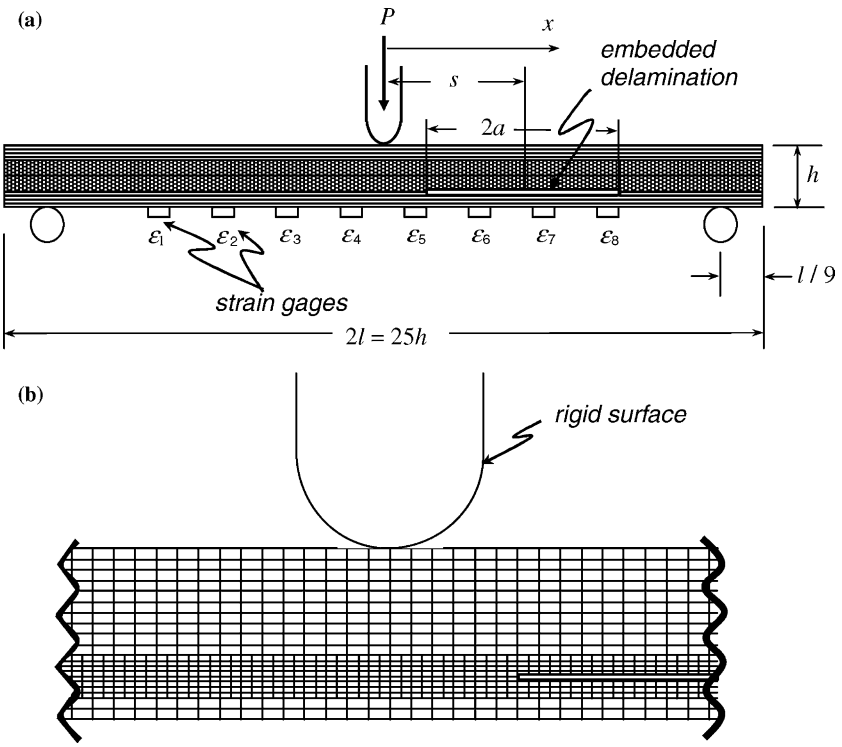

Figure 2. (a) Schematic of $[0/90]_s$ laminate containing an embedded interlaminar delamination subjected to three-point-bend. Vertical scales are magnified by two times for clarity. (b) Finite element mesh near the load-point.

located in the general vicinity of one another, the present method is likely to be ineffective in its estimations.

In the four-ply model, the laminate thickness is denoted as h while the length is set as $2l(=25h)$. In each ply, the material is assumed to be transversely isotropic and their linear anisotropic properties are $E_L = 125\,\text{GPa}$, $E_T = 8.50\,\text{GPa}$, $\nu_{LT} = 0.330$, $\nu_T = 0.176$ and $G_{LT} = 4.7\,\text{GPa}$, respectively. Here the subscript 'L' indicates the fiber direction while the subscript 'T' indicates the transverse direction. The laminate is subjected to three-point-bend loading as shown in Figure 2a. If an interlaminar delamination exists, it should be reflected upon axial strains due to increased compliance. The effect of delamination in composite laminate can be also observed under uniaxial compression. However such an effect is minimal when the load is less than the buckling load. Furthermore, the delamination has no effect on buckling load if its length is less than 20% of laminate length, which is usually many multiples of thickness (Wu et al., 1998). The axial strains are measured at discrete surface locations on the opposite side of the load application as shown. In the analysis, the total number of gages is set eight although any number of gages can be accommodated in the present procedure. In general, required number of gages is dictated by the gage spacing and the total span of laminate that needs to be inspected. The gages in the present model are spaced $2h$ apart and the strain measurements are denoted as $\varepsilon_1 \sim \varepsilon_8$, respectively. The gage spacing should be set according to the minimum delamination size to be identified. With large gage spacing, it would be difficult to detect small delaminations whereas small spacing will require more gages. Regardless, it is difficult to detect delaminations that are less than the laminate thickness ($2a/h < 1$) since such delaminations do not influence the deformation characteristics. However, in general, small flaws are not immediately detrimental to the structural integrity, as long as they are detected before they grow to critical sizes.

In the present verification analysis, finite element calculations are carried out to generate simulated strain measurements. The radii of the loading pin as well as the support pins are chosen as $0.5h$. Figure 2b shows an enlarged portion of the finite element mesh. An automatic mesh generator code was developed to construct models with various delamination sizes and locations. Along the delamination, contact conditions are enforced to prevent surface overlapping. A typical model contains about 5600 four-noded generalized plane strain isoparametric elements. Here, smaller elements are placed near the interface of the 3rd and 4th layer to accommodate higher stresses near the delamination.

2.2. Delamination-deformation relation

Existence of interfacial delamination can influence the deformation behavior of the laminate. The exact nature of delamination–deformation relation is very complex and a closed form solution is not generally available. However, so-called forward solutions are still needed to search for the best estimates. Here, finite element calculations are carried out to establish the delamination–deformation relation for various delamination sizes and location. In an iterative type of inverse analysis such as this, the forward solutions are referenced during updating. If calculations were performed for each estimate, the total number of calculations would be very large, and such a process would be prohibitively time-consuming. To circumvent this difficulty,

a feasible approach is adopted in the present procedure. A reference/forward solution that relates the delamination parameters to measured parameters is established prior to the error minimization process. A number of finite element calculations are carried out for discrete combinations of delamination location and size to determine corresponding strains and deflections. To approximate the strains and deflection at other combinations of s and $2a$, bilinear interpolation functions are utilized. With this approach, the total number of required computations is kept at a reasonable level. The axial strain at αth strain gage, $\varepsilon_\alpha(s, 2a)$, is expressed as a continuous function of the delamination parameters as

$$\varepsilon_\alpha(s, 2a) \approx \sum_{i=1}^{p} \sum_{j=1}^{q} \varepsilon_\alpha(s_i, 2a_j) N_{ij}(s, 2a). \tag{1}$$

Here, s_i is the ith sample point within the range of delamination location, $2a_j$ is the jth sample point within the range of delamination size, and N_{ij} is the corresponding bilinear interpolation function. In this study, the range of values for delamination location is $-7 \leqslant s/h \leqslant 7$ while for delamination size, it is $1.38 \leqslant 2a/h \leqslant 5.50$. In actual applications, these ranges should be selected according to the delamination size considered to be critical and the span of laminate to be inspected. The values of $\varepsilon_\alpha(s_i, 2a_j)$ in (1) are obtained from performing various finite element calculations. In the calculations, 15 different values (equally incremented) for the delamination location and 12 different values (equally incremented) for the size are selected. Thus, total of 180 separate models are constructed and computed. Several other increments were also tested and it was found that these intervals provide sufficiently smooth and accurate functions of strains. Similar interpolation functions are also used for the deflection.

To illustrate an effect of delamination, the strain at the 3rd gage located at $x/h = -3$ is shown as a function of delamination size and location (i.e., $\varepsilon_3(s, 2a)$) in Figure 3. Here, the strain is normalized by the reference strain ε^{ref}, which corresponds to the strain without delamination. A pronounced effect of delamination is

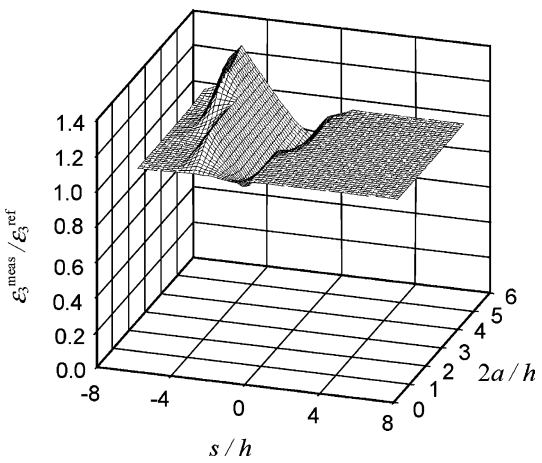

Figure 3. Normalized strain at the 3rd gage for various delamination sizes and locations. Peaks and valleys represent effects of delamination location and size.

observed when it is in the vicinity of the gage ($x/h = -3$). Also the deviation from the reference strain generally increases with the delamination size. However, as expected, when the delamination is away from the gage, essentially no effect is observed. The flat plateau on the three-dimensional surface is an indication of no effect of delamination on this strain gage. These results clearly suggest not only that gages near the delamination can detect the existence of flaw but also the importance of proper gage spacing.

2.3. Error objective function

In order to extract the unknown parameters, the present procedure minimizes the difference between the *actual measurements* of strains and the strains corresponding to *estimated* delamination parameters. If s^{est} and $2a^{\text{est}}$ are the estimated delamination location and delamination size, respectively, then the error objective function for n strain measurements can be formulated as

$$\Phi(s, 2a) = \frac{1}{n} \sum_{\alpha=1}^{n} \left(\frac{\varepsilon_\alpha(s^{\text{est}}, 2a^{\text{est}}) - \varepsilon_\alpha^{\text{meas}}}{\varepsilon_\alpha^{\text{ref}}} \right)^2 . \tag{2}$$

Initially, the number of strain measurements is selected as $n = 8$. The minimization of this objective function should lead to the best estimation of delamination parameters. The search for the best estimates is performed with the downhill simplex method for multivariate problems as discussed next.

2.4. Downhill simplex method

The downhill simplex method was originally proposed by Nelder and Mead (1965). It is one of the more popular multi-dimensional optimization methods when derivatives of objective function are either unavailable or discontinuous. The computational strategy involved in this method is unique in comparison to other multi-dimensional algorithms since it is self-sustained and does not make use of any one-dimensional algorithm as a part of its procedure (Press et al., 1992). However, potential disadvantage of this method includes possibility of collapse in convergence process as the method might terminate prematurely at a steep valley (Jacoby et al., 1972). Choosing a large number of initial guesses can usually circumvent this problem as implemented in the present approach.

The downhill simplex method can find solution in an infinite domain although the present problem will have a finite domain. In the case of an optimization problem with m unknown parameters, the number of vertices of a simplex is $m + 1$. With two unknown parameters here, the shape of simplex is a triangle for the optimization process and a simplex is defined through three points or sets of estimates. The first point can be chosen arbitrarily within the domain. The other two points are chosen in such a manner that they enclose a non-degenerate area. As noted earlier, since some estimates might get trapped in valleys (i.e., local minima), it is necessary to choose many different sets of initial estimates. In the present analysis, the number of initial points chosen is $729 (= 27 \times 27)$ within the domain. The three vertices forming the initial simplex are adjacent to each other and form a right-angled triangle. The method searches

for minima of the function by making a series of moves. Details of the downhill simplex method are described in Appendix A. The search process terminates when the step size becomes very small or when the number of iterations reaches 1000.

3. Verification study

3.1. Identification with strain measurements

Initially, only strain measurements under three-point-bend load applied at the mid-span of the model were used to determine the unknown parameters. For the verification of the proposed approach, the delamination parameters were set as $s/h = 1.75$ and $2a/h = 3.50$, respectively. After the finite element calculation, simulated strain measurements were supplied as the input to the inverse method. The corresponding computed strains $\varepsilon_1, \varepsilon_2, \ldots, \varepsilon_8$ are normalized and shown in Figure 4a. As predicted, the gages numbers 5 and 6 (at $x/h = 1$ and 3) show large deviations from the reference strain as they are close to the delamination location. However, other

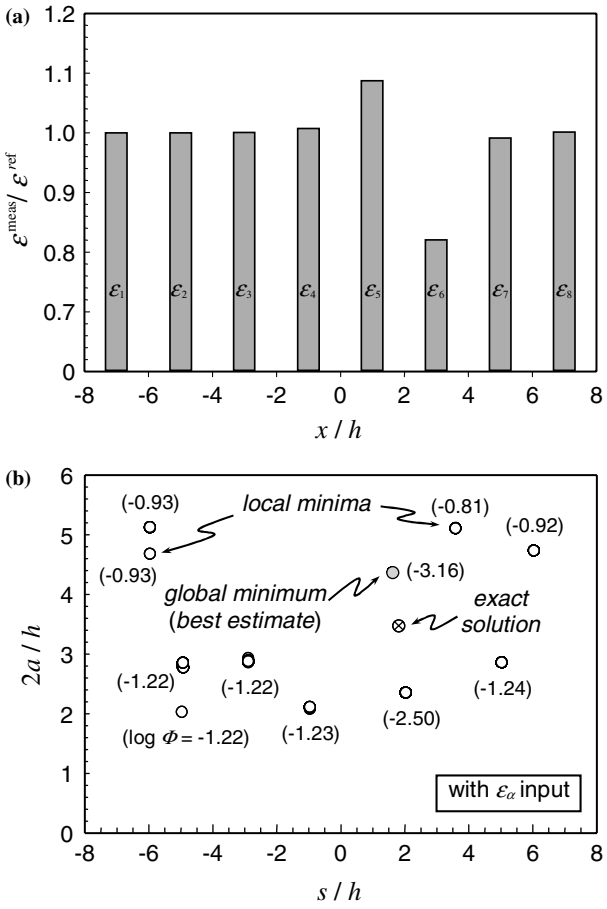

Figure 4. (a) Normalized strain at eight locations under three-point bend for $s/h = 1.75$ and $2a/h = 3.50$. (b) Local and global minima are shown in the domain of unknown parameters. At each point, corresponding log Φ value is noted. Exact solution is also shown for reference.

strains are almost identical to the reference strain. With these results as input, the error objective function in (2) is minimized with the downhill simplex method.

The results are shown in Figure 4b. Here, 729 initial points are chosen and the downhill simplex method is performed for each case. The figure shows locations where different initial points converged. These converged locations are termed as local minima and shown with open circles. These locations also represent valleys where the estimates get trapped. Note each circle contains many different initial estimates. In order to identify the global minima and best estimates, the value of the objective function (2) is computed at each local minimum. Note one cannot compare total numbers of initial estimates converged at local minima to determine the global minimum. In the figure, logarithmic value of objective function is noted at each local minimum. The point having the smallest log Φ is labeled as the global minimum. Its location in terms of s/h and a/h are chosen as the best estimates of unknown parameters. In the figure, the global minimum, shown with a shaded circle, has the values of $s/h = 1.6$ and $2\ a/h = 4.4$, respectively (exact/input values are $s/h = 1.75$ and $2\ a/h = 3.50$). Although the estimate of delamination location can be acceptable, the estimated size is not satisfactory. The main cause for this error can be attributed to the functional dependence of strains on the delamination parameters. From many finite element calculations for various values of s and $2a$, it was observed that strains were strong functions of delamination location but generally weak functions of delamination size. Hence, strain measurements alone cannot yield accurate predictions for delamination size. An improved procedure for better estimation is described next.

3.2. Identification with strain and deflection measurements

In order to improve the estimates, it is necessary to find an additional measurement, which is sensitive to the delamination size. It is also important that such a measurement be obtained without a significant increase in experimental effort. In view of these, the deflection at loading-point is tried as an additional input in the identification process. With an instrumented tensile machine, the deflection can be simultaneously obtained in the three-point-bend test performed to measure strains. With such an additional input, the objective function is then modified as

$$\Phi(s, 2a) = \frac{1}{n} \sum_{\alpha=1}^{n} \left(\frac{\varepsilon_\alpha(s^{\text{est}}, 2a^{\text{est}}) - \varepsilon_\alpha^{\text{meas}}}{\varepsilon_\alpha^{\text{ref}}} \right)^2 + \left(\frac{\delta(s^{\text{est}}, 2a^{\text{est}}) - \delta^{\text{meas}}}{\delta^{\text{ref}}} \right)^2. \tag{3}$$

Here, δ^{ref} is the reference deflection when the laminate contains no delamination. Here, the forward solutions, $\delta(s^{\text{est}}, 2a^{\text{est}})$, is constructed in a similar manner as the strains from finite element calculations. The deflection of the loading pin at the center for various combinations of delamination locations s and lengths $2a$ is shown in Figure 5. Except near $s/h = 0$, the slope of surface is steep along $2a/h$, which indicates the deflection to be a strong function of the delamination size. Hence, the combined inputs of strains and deflection should improve the estimates.

To examine the accuracy, delamination parameters with $s/h = 1.75$ and $2a/h = 3.50$ were again tested. For this model, the deflection at load point was computed as $\delta^{\text{meas}}/\delta^{\text{ref}} = 1.039$. This additional information is supplied in the objective function (3), and Φ is minimized with the downhill simplex method. The local and global

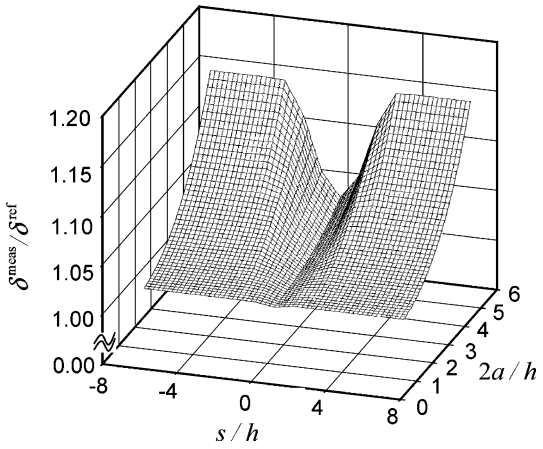

Figure 5. Normalized deflection at load-point for various delamination sizes and locations. The surface variation implies a strong dependence on delamination size (i.e., $2a/h$).

minima obtained are shown in Figure 6. A notable improvement is the reduction in scatter for the local minima. This suggests that greater numbers of initial points have converged to a fewer minima than those in the previous case. The best estimates corresponding to the global minimum were identified as $s/h = 1.4$ and $2a/h = 4.0$, respectively. These values are incremental improvement over the previous estimates. Note, however, for some other values of s/h and $2a/h$, tested, greater improvements are observed with the additional deflection input. In fact, the accuracy of the estimates is not constant with different values of delamination parameters (see Section 4 for the error sensitivity analysis). Furthermore improvements are still needed for the proposed approach to be effective for any values of delamination parameters.

3.3. Identification with measurements under multiple loading conditions

An importance factor in the proposed identification method is to keep required measurement process as simple as possible. In this method, a major effort must be

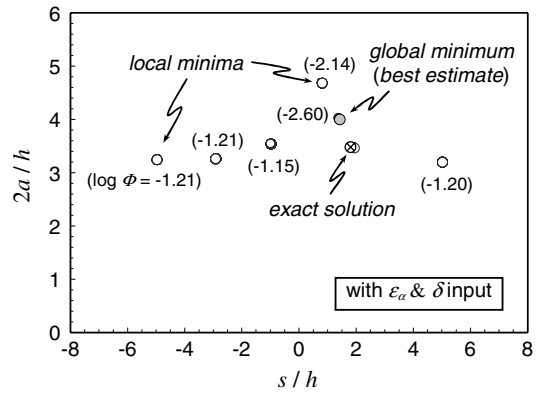

Figure 6. Local and global minima are shown in the domain of unknown parameters (with exact values, $s/h = 1.75$ and $2a/h = 3.50$). They were obtained with eight strain measurements and a deflection measurement. At each point, corresponding $\log \Phi$ value is noted.

consumed for bonding of various strain gages. However, so-called strip gage, which usually has 10 equally spaced gages, is available today. With this gage, only a single bonding of the strip is required. Regardless, once the gages are attached, strains under different loading conditions can be found relatively easily. Hence, additional loadings are considered to provide additional measurements in the inverse analysis. Although these additional inputs may not offer substantially new information to the inverse analysis, they can still improve the estimates. Figure 7 shows a schematic of three-point bend with loading at the center, left and right of the model. The first case corresponds to the initial load case while the latter two cases are additional load cases. They are denoted as load cases 1, 2 and 3, respectively. Altogether, three separate loadings are carried out to measure strains and deflections with the total of 24 strain and 3 deflection measurements.

With these measurements, the objective function is once again modified. The new objective function for m different loading conditions can be expressed as

$$\Phi(s,2a)=\frac{1}{n\times m}\sum_{\alpha=1}^{n}\sum_{\beta=1}^{m}\left(\frac{\varepsilon_{\alpha\beta}(s^{\text{est}},2a^{\text{est}})-\varepsilon_{\alpha\beta}^{\text{meas}}}{\varepsilon_{\alpha\beta}^{\text{ref}}}\right)^2+\frac{1}{m}\sum_{\beta=1}^{m}\left(\frac{\delta_{\beta}(s^{\text{est}},2a^{\text{est}})-\delta_{\beta}^{\text{meas}}}{\delta_{\beta}^{\text{ref}}}\right)^2. \tag{4}$$

Here, the number of loading conditions is $m=3$, and the subscript 'β' represents the loading case. Additional finite element calculations were also performed to establish reference solutions for the two additional cases.

The simulated strains under three different loading conditions are shown in Figure 8a. As predicted, only ε_5 and ε_6 (measured at $x/h=1$ and 3) still showed deviations from the reference strain. However it is interesting to note the strain change under load case 3 was very different from those under load cases 1 and 2. The physical explanation is that the loading point of case 3 is located right while the loading points of cases 1 and 2 is located left of the delamination, which result in reverse strain behaviors at gages 5 and 6. The normalized deflections under three loading conditions were $\delta_1^{\text{meas}}/\delta^{\text{ref}}=1.039$, $\delta_2^{\text{meas}}/\delta^{\text{ref}}=1.017$ and $\delta_3^{\text{meas}}/\delta^{\text{ref}}=1.017$, respectively. As previously noted, these results suggest that the deflection is nearly indifferent to the delamination location unless the delamination is located in close vicinity of the loading point.

Using these measurements, the objective function (4) is minimized with the downhill simplex method. The resulting local and global minima are shown in Figure 8b. With these additional inputs, the total number of local minima further decreased

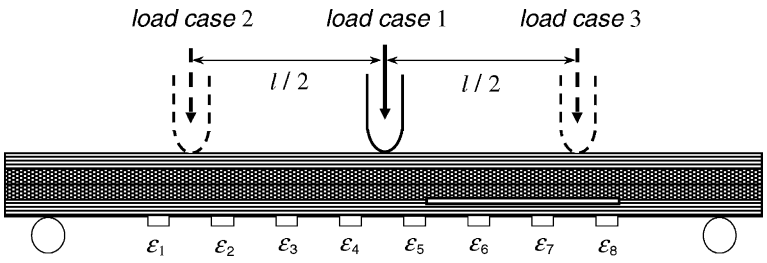

Figure 7. Schematic of four ply [0/90]$_s$ laminate under three different loading conditions. The loading at the center, left and right are termed as load cases 1, 2 and 3, respectively.

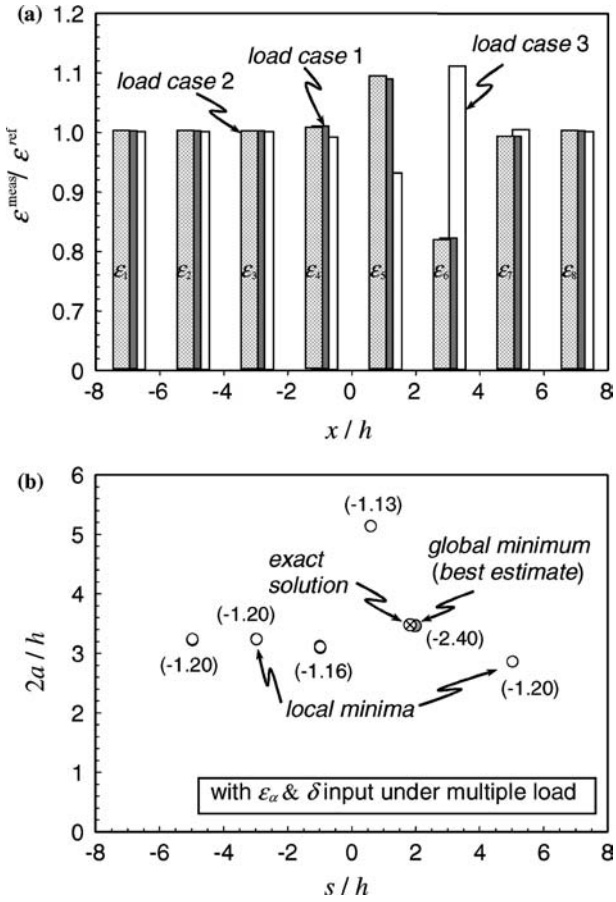

Figure 8. (a) Normalized strains for $s/h = 1.75$ and $2a/h = 3.50$. (b) Local and global minima are shown in the domain of unknown parameters. They were obtained with 24 strain and 3 deflection measurements. At each point, corresponding $\log \Phi$ value is noted.

and the global minimum approached very close to the exact solutions. The best estimates at this location is $s/h = 1.9$ and $2a/h = 3.5$ (with exact values $s/h = 1.75$ and $2a/h = 3.50$). These results confirmed the improvements of estimates with the additional measurements and the effectiveness of proposed inverse procedure to identify the unknowns. As previously noted, the convergence behavior varies with different values of delamination parameters. Furthermore, actual experimental measurements always contain some errors. Thus, for this method to be robust, it must be able to determine accurate estimates under various conditions. These aspects are studied in the next section.

4. Error sensitivity analysis

In general, estimates of an inverse analysis are influenced by measurement errors. In order to assess the robustness of inverse analysis approach, its ability to estimate the parameters with presence of measurement errors must be evaluated. Examples of error sources for strain measurements include misalignment of gages and

imperfections introduced while bonding. Also, actual gages record a strain averaged over the area it occupies. In the current analysis, pointwise strain measurements are considered. Although the averaged strains can be easily used in the reference solutions, if deviations arising from the averaging are small, this effect can be included as one factor in the error sensitivity analysis shown here. Since the strain variation over any single gage should be approximately linear, we expect any deviations to be very limited (say within $\sim$1%).

In the detailed error sensitivity analysis, *simulated measurements* were perturbed with additions of small values determined randomly. The maximum bound of errors in the strain measurements are set as $\pm 2\%$ while $\pm 1\%$ is used for the deflection measurements. A smaller measurement tolerance is assumed for the deflection since it generally provides more accurate results than those of strain. Within these ranges, randomly generated errors are artificially added to the originally computed strains and deflections. Since a single modified case does not elucidate the overall characteristics of error sensitivity, 50 different cases with different sets of error perturbations were analyzed. For each case, the inverse method was performed as described in Section 3. First, local minima are determined, and then global minimum with the lowest value of objective function is identified. This process is repeated 50 times for each model presented here.

First, the error analyses are carried out for the procedure described in Section 3.1 to confirm that unsatisfactory results with just eight strain measurements are not unique. Figure 9a shows the global minima represented by the gray circles for 50 different cases. The local minima of each case are not shown here for clarity. None of these global minima is close to the exact solutions as shown in the figure. This proves that strain measurements alone cannot yield accurate estimations.

Next, the error sensitivity analysis is carried out with the improved identification procedure described in Section 3.3. In the result shown in Figure 8b without error, almost exact values are estimated with 24 strain and 3 deflection measurements. Here 50 separate sets of measurements are generated with additions of random errors. The global minimum of each case is shown in Figure 9b. Although there is still a small scatter along the range of delamination length, all of the global minima are well contained close to the exact values. This result should support the robustness of the present method to estimate the unknown delamination parameters.

The convergence behavior is also influenced by particular values of delamination sizes and locations. For completeness, the error sensitivity analysis was performed for different sets of delamination parameters. First, a model with $s/h = -3.38$ and $2a/h = 4.25$ was considered. Similar computations are carried to generate simulated measurements. Then random errors are added to these measurements and the downhill simplex method was performed for 50 different cases. The resulting global minima are shown in Figure 10a. The global minima are clustered in a small domain very close to the exact solution. This shows that highly accurate estimates are obtained even with the measurement errors. Another model with different parameters was also examined. Here they are chosen as $s/h = 4.50$ and $2a/h = 2.88$, respectively, and their global minima are shown in Figure 10b. In this model, the global minima are somewhat more spread around the exact solution. The increased scatter is due to the smaller size of delamination. In smaller delamination models, the relative magnitudes of added errors with respect to the strain deviation ($|\varepsilon^{\text{meas}} - \varepsilon^{\text{ref}}|$) and deflection

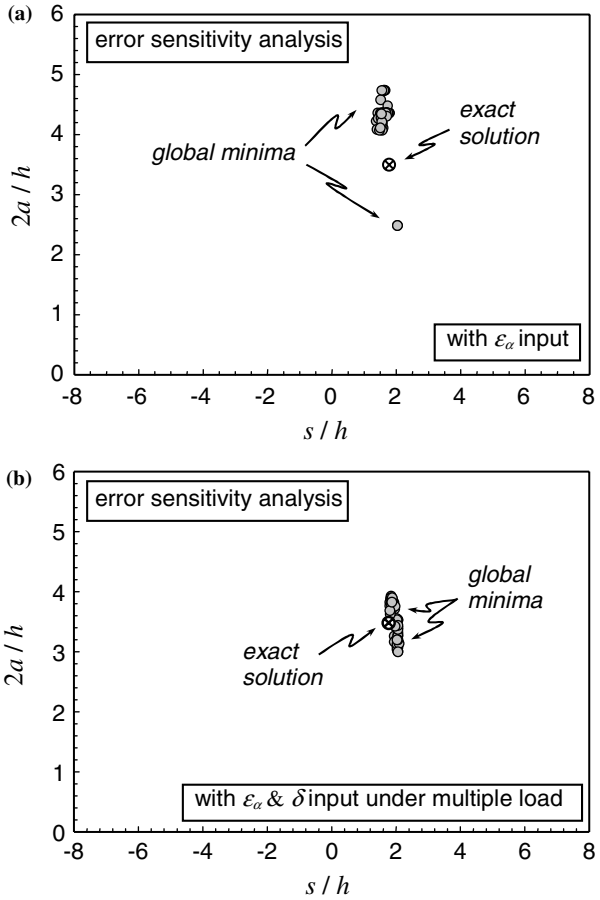

Figure 9. Global minima determined in the error sensitivity analysis are shown for $s/h = 1.75$ and $2a/h = 3.50$. Here 50 separate analyses (with different random errors added to measurements) are performed in each model. (a) Identification with eight strains. (b) Identification with 24 strains and eight deflections.

deviation are greater. Thus, one would observe greater error. Nevertheless, the scatter is still well contained even for the small delamination. Although, in actual implementation of the method, other sources of error must be accounted, the error sensitivity analysis supports the effectiveness of the proposed procedure. Other values of delamination parameters were also tested but not shown due to page limitation. Although, some differences in the scattering behaviors were observed, general trends were consistent with the models presented here.

5. Discussions

A novel approach based on an inverse analysis technique was proposed to identify embedded interlaminar delamination in composite panels. The scheme was developed as an alternative approach to more costly flaw detection techniques. Surface strains and deflections resulting from bending tests were chosen as possible measurements. Applicability of a stochastic procedure, 'downhill simplex method' was demonstrated as a potential tool in the identification of unknown delamination parameters. In

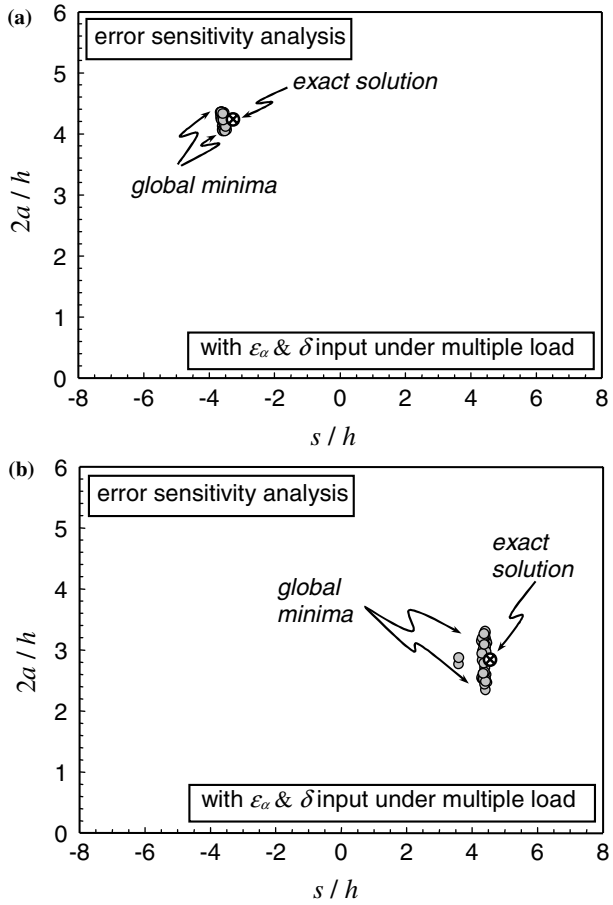

Figure 10. Global minima determined in the error sensitivity analysis are shown in the domain of unknown parameters. For each multiple loading case, 50 separate analyses (with different random errors added to measurements) are performed. (a) Identification with $s/h = -3.38$ and $2a/h = 4.25$. (b) Identification with $s/h = 4.50$ and $2a/h = 2.88$.

the verification analysis, four-ply laminate is used as the test model and simulated measurements are obtained for different values of delamination size and location. Improvements in the procedure are made during this analysis. When strain and deflection measurements obtained from three different loading conditions are used, the proposed procedure yielded accurate estimates. The steps of the current inverse analysis procedure are outlined in Figure 11. Key features of this approach can be described as follows:

1. In order to construct forward/reference solutions *a priori*, measurable parameters are constructed as approximate and continuous functions of unknown delamination parameters using finite element calculations and interpolation functions. This approach reduces the computational cost during the search process.
2. The error objective function that expresses the accuracy of estimates is clearly established.
3. The downhill simplex method is utilized to search values corresponding to the minimal objective function. The technique is very effective when gradients of objective function are not available.

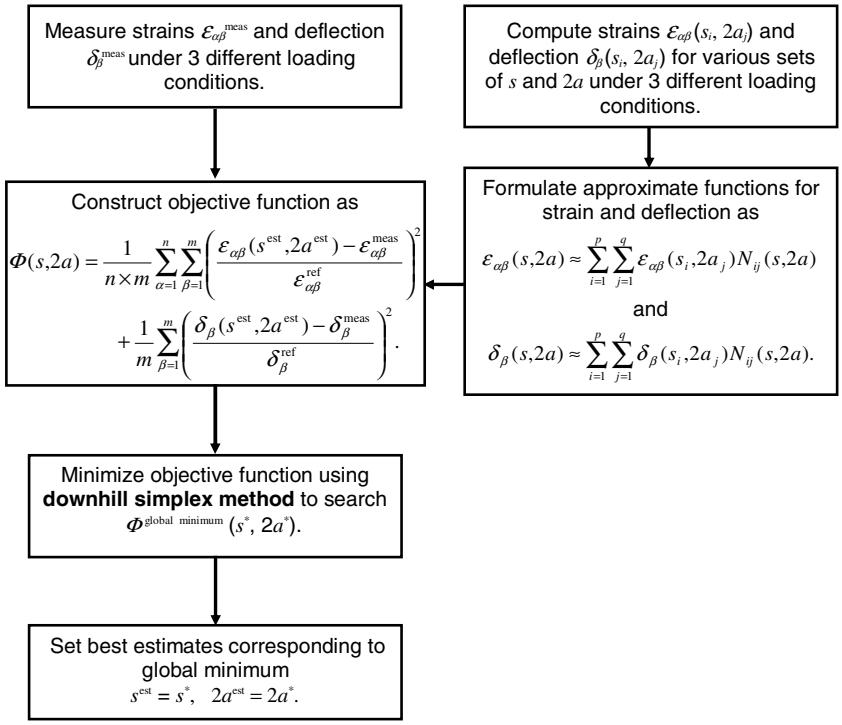

Figure 11. Outline of inverse analysis procedure to identify unknown parameters.

4. In order to improve the estimates with minimal additional efforts, strain and deflection measurements under multiple loadings conditions are included in the identification process.
5. The error sensitivity study confirms the robustness of the proposed method even with expected measurement errors.

Prior to implementing this procedure in actual experiments, it is important to clarify some limitations. First, the model assumes only single delamination to exist. In reality, multiple delaminations might exist both along the same ply interfaces and across different interfaces. When the delaminations are across different ply interfaces at nearly same locations, the proposed method should be still effective although the estimates will show up as a larger delamination at about the same location. If multiple delaminations are at different in-plane locations, then the current method cannot uncouple their responses although the general locations of delaminations can still be detected from strain measurements. Second, the proposed method does not assume other types of damage in the composite (e.g., surface degradation due to environment). If they are present, strain and deflection measurements may be affected. Third, the present verification study was performed for two-dimensional through-delamination model. However, in actual composite laminate, flaws may be entirely embedded. The proposed method can be extended with proper modifications in such cases. However, more complex three-dimensional study will be required and strain measurements must be made over a surface instead of along a line. Obviously the number of unknowns would increase (e.g., $2a_x$, $2a_y$, s_x and s_y) and more efforts will

be needed to obtain accurate estimates since the deflections would be less sensitive to entirely embedded delaminations. A further study will be required to assess the robustness of such a procedure.

In addition to the downhill simplex algorithm, an alternate minimization algorithm was also tested for potential applicability. Here, a genetic algorithm, which was inspired by the evolution theory proposed by Darwin, was examined. The algorithm operates on a given population of m chromosomes (estimates – s_i and $2a_i$, where $i = 1, 2, \ldots, n$). Then, a new population is generated by performing four steps namely, selection, crossover, mutation and replacement, and the fitness is evaluated at each estimate. A new generation (iteration) is populated until the termination criterion is achieved. In this problem, m was chosen as 30 after trials and the criterion was set as, $|\Phi_{\min}(s^{n+1}, 2a^{n+1}) - \Phi_{\min}(s^n, 2a^n)|/\Phi_{\min}(s^n, 2a^n) \leqslant 1 \times 10^{-7}$. Here $\Phi_{\min}(s^n, 2a^n)$ represents the lowest fitness/objective function value in nth iteration. Convergence was achieved generally after 100 iterations. For the cases with 24 strain and 3 deflection measurements, the estimates were almost identical to ones determined with the downhill simplex method. One potential advantage of genetic algorithms is that *mutation* steps of the algorithm take care of avoiding local minima. However, the genetic algorithm takes a longer time (roughly 10 times) to converge to the solutions. Further details about genetic algorithms can be found in Goldberg et al. (1989).

Acknowledgements

The authors gratefully acknowledge the Army Research Office for their support under DAAD19-02-1-0333. The computations were carried out using finite element code ABAQUS, which was made available under academic license from Hibbitt, Karlsson and Sorensen Inc.

References

Aymerich, F. and Meili, S. (2000). Ultrasonic evaluation of matrix damage in impacted composite laminates. *Composites Part B* **31**, 1–6.

Frederiksen, P.S. (1997). Experimental procedure and results for the identification of elastic constants of thick orthotropic plates. *Journal of Composite Materials* **31**, 360–382.

Goldberg, D.E. (1989). *Genetic Algorithms in Search, Optimization and Machine Learning*. Addison-Wesley Longman publishing company.

Grady, J.E. and Sun, C.T. (1986). Dynamic delamination crack propagation in graphite/epoxy laminate. In: *Composite Materials: Fatigue and Fracture*, ASTM STP 907 (Edited by Hahn, H.T.), Philadelphia, 5–31.

Ishak, S.I., Liu, G.R., Shang, H.M. and Lim, S.P. (2001). Locating and sizing of delamination in composite laminates using computational and experimental methods. *Composites Part B: Engineering* **32**, 287–298.

Jacoby, S.L.S., Kowalik, J.S., Pizzo, J.T. and Veterling, W.T. (1972). *Iterative Methods for Nonlinear Optimization Problems*, Prentice-Hall, Englewood Cliffs.

Leung, C.K.Y., Yang, Z., Tong, P., Xu, Y. and Lee, S.K.L. (2001). A new fiber optic-based method for delamination detection in composites. *Proceedings of 3rd International Workshop on Structural Health Monitoring: The Demands and Challenges* (Edited by Chang, F.K.), CRC Press, Stanford CA, 1209–1216.

Liu, G.R. and Chen, S.C. (2001). Flaw detection in sandwich plates based on time-harmonic response using genetic algorithm. *Computer Methods in Applied Mechanics and Engineering* **190**, 5505–5514.

McCann, D.M. and Forde, M.C. (2001). Review of NDT methods in the assessment of concrete and masonry structures. *NDT & E International* **34**, 71–84.
Mook, G., Lange, R. and Koeser, O. (2001). Non-destructive characterisation of carbon-fibre-reinforced plastics by means of eddy-currents. *Composites Science and Technology* **61**, 865–873.
Nakamura, T., Kushner, A. and Lo, C.Y. (1995). Interlaminar dynamic crack propagation. *International journal of solids and structures* **32**, 2657–2675.
Nelder, J.A. and Mead, R. (1965). A simplex method for function minimization. *Computer Journal* **7**, 308–313.
Press, W.H., Teukolsky, S.A., Vetterling, W.T. and Flannery, B.P. (1992). *Numerical recipes in C: The Art of Scientific Computing*, Cambridge University Press.
Sakagami, T. and Ogura, K. (1994). New flaw inspection technique based on infrared thermal images under joule effect heating. *JSME International Journal* Series A **37**, 380–388.
Sun, C.T. and Manoharan, M.G. (1989). Growth of delamination cracks due to bending in a $[90_5/0_5/90_5]$ laminate. *Composites Science and Technology* **34**, 365–377.
Tan, P. and Tong, L.A. (2004). Delamination detection model for composite beams using PFRC sensor/actuator. *Composites Part A: Applied Science and Manufacturing* **35**, 231–247.
Tarantola, A. (1987). *Inverse Problem Theory: Methods for Data Fitting and Model Parameter Estimation*. Elsevier Inc., New York.
Todoroki, A. (2001). The effect of number of electrodes and diagnostic tool for monitoring the delamination of CFRP laminates by changes in electrical resistance. *Composites Science and Technology* **61**, 1871–1880.
Wang, S.S., Suemasu, H. and Zahlan, N.M. (1984). Interlaminar fracture of random short-fiber SMC composite. *Journal of Composite Materials* **18**, 574–594.
Wu, L.C., Lo, C.Y., Nakamura, T. and Kushner, A. (1998). Identifying failure mechanisms of composite structures under compressive load. *International Journal of Solids and Structures* **35**, 1137–1161.
Xu, Y.G., Liu, G.R., Wu, Z.P. and Huang, X.M. (2001). Adaptive multilayer perceptron networks for detection of cracks in anisotropic laminated plates. *International Journal of Solids and Structures* **38**, 5625–5645.
Yan, Y.J. and Yam, L.H. (2004). Detection of delamination damage in composite plates using energy spectrum of structural dynamic responses decomposed by wavelet analysis. *Computers and Structures* **82**, 347–358.

Appendix A

The downhill simplex method minimizes the objective function by taking a series of steps. The shape of the simplex chosen here is a triangle defined by a set of three points. Suppose $\boldsymbol{p}_1$, $\boldsymbol{p}_2$ and $\boldsymbol{p}_3$ are denoted as three points on s–a plane and the objective functions at these points are such that $\Phi(p_1) < \Phi(p_2) < \Phi(p_3)$, where $\boldsymbol{p}_1 = (s_1, 2a_1)$, $\boldsymbol{p}_2 = (s_2, 2a_2)$ and $\boldsymbol{p}_3 = (s_3, 2a_3)$ corresponding to three different delamination parameters. The four types of steps are outlined below.

Step 1: Reflection – Most of the steps in a Downhill Simplex Method are reflections. This step moves the *highest point* (where the value of objective function is larger than at the other two points) through the opposite face of the simplex to a supposedly *lower point* (where the value of the objective function is expected to be lower than at the *highest point*), thereby flipping the triangle by 180°. This step is performed in an attempt to move the triangle closer to the exact solution of the problem. The reflected point ($\boldsymbol{p}_r$) is found as

$$\boldsymbol{p}_r = 2\boldsymbol{p}_m - \boldsymbol{p}_3. \tag{A1}$$

Here, $\boldsymbol{p}_m = (\boldsymbol{p}_1 + \boldsymbol{p}_2)/2$. Note that the *highest point* here is $\boldsymbol{p}_3$. The objective function evaluated at the reflected point is $\Phi_r = \Phi(\boldsymbol{p}_r)$.

Step 2: Reflection and expansion – The second type of move is termed as reflection and expansion. This is performed when the value of objective function further drops along the line of reflection of the *highest point*. This step is designed to further accelerate the process of convergence. The corresponding point ($\boldsymbol{p}_e$) is

$$\boldsymbol{p}_e = \boldsymbol{p}_r + (\boldsymbol{p}_m - \boldsymbol{p}_3). \tag{A2}$$

The objective function evaluated at this point is $\Phi_e = \Phi\ (\boldsymbol{p}_e)$.

Step 3: Contraction – Moving the highest *point* in an attempt to decrease the area enclosed by the simplex, yields a third move termed contraction. This step is usually performed when reflection of the highest point does not cause further decrease in the value of the objective function. The idea here is that the local minimum lies within the triangle. The point corresponding to contraction ($\boldsymbol{p}_c$) is

$$\boldsymbol{p}_c = (\boldsymbol{p}_m + \boldsymbol{p}_3)/2. \tag{A3}$$

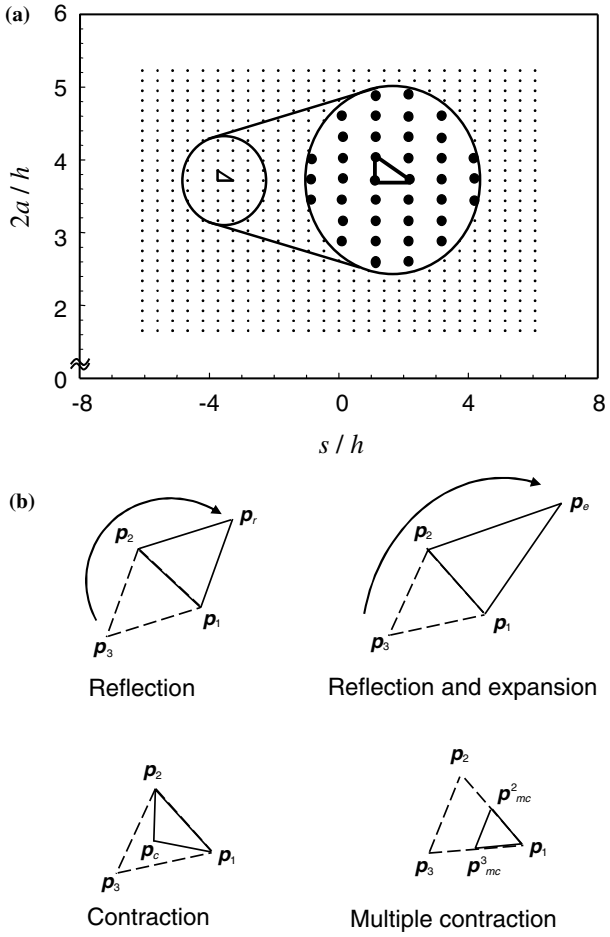

Figure A1. (a) Initial points to perform the downhill simplex method. An enlarged right-angled triangle that is the typical shape and size of the initial simplex is shown. (b) Possible moves of downhill simplex method in the domain of unknown parameters. The points are arranged so that the values of objective functions are $\Phi(\boldsymbol{p}_1) < \Phi(\boldsymbol{p}_2) < \Phi(\boldsymbol{p}_3)$.

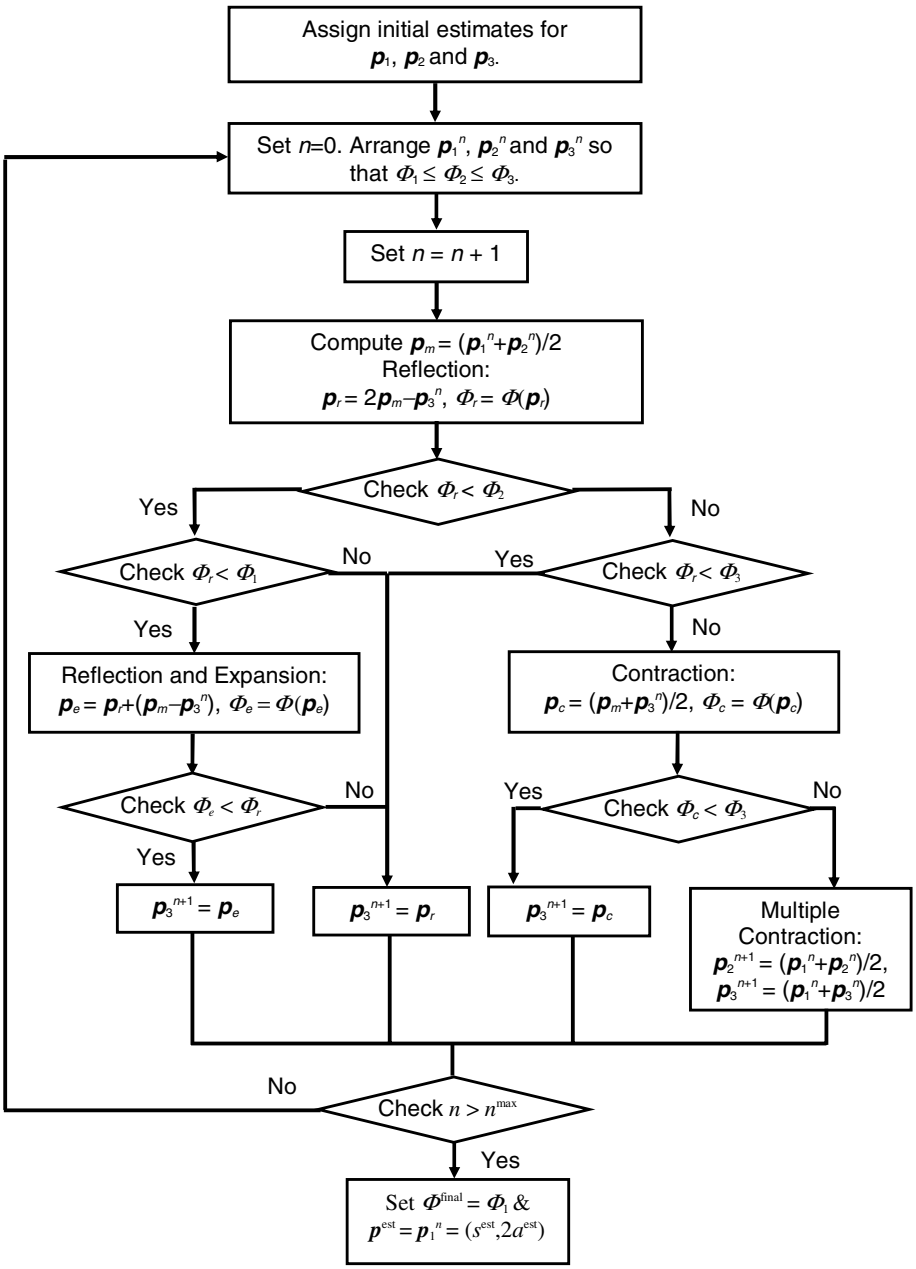

Figure A2. Flowchart for the downhill simplex method.

The objective function evaluated at this point is $\Phi_c = \Phi(\boldsymbol{p}_c)$.

Step 4: Multiple Contraction – The fourth move called multiple contraction occurs when all vertices of the simplex pull around its *lowest point* (Press et al., 1992). This is performed when contraction does not cause a decrease in the objective function of the point under consideration. The *lowest point* here is $\boldsymbol{p}_1$. So, there are two new points to be evaluated here. Let them be denoted as $\boldsymbol{p}_{\text{mc}}^2$ and $\boldsymbol{p}_{\text{mc}}^3$. They are found as

$$\boldsymbol{p}_{\text{mc}}^2 = (\boldsymbol{p}_1 + \boldsymbol{p}_2)/2 \quad \text{and} \quad \boldsymbol{p}_{\text{mc}}^3 = (\boldsymbol{p}_1 + \boldsymbol{p}_3)/2. \tag{A4}$$

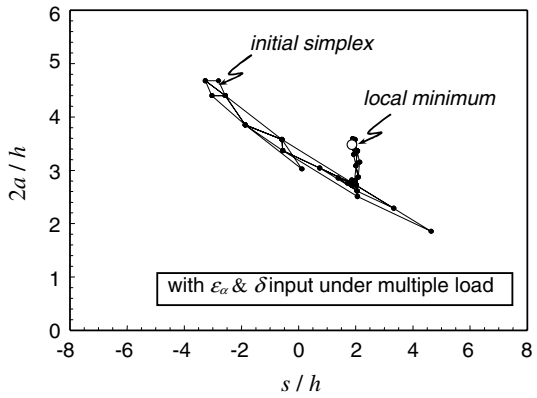

Figure A3. Movement of simplex for the $s/h = 1.75$ and $2a/h = 3.50$ case. The location of the initial simplex is noted. Local minimum after performing the downhill simplex method is highlighted.

The objective functions evaluated at the two points are $\Phi^2_{\mathrm{mc}} = \Phi(\boldsymbol{p}^2_{\mathrm{mc}})$ and $\Phi^3_{\mathrm{mc}} = \Phi(\boldsymbol{p}^3_{\mathrm{mc}})$. The initial points chosen in this study for performing the downhill simplex method are illustrated in Figure A1a. Here, a total of $729 = 27 \times 27$ points are chosen along the range of delamination location s and delamination size $2\ a$. The various types of steps are geometrically shown in Figure A1b. The complete flowchart of the downhill simplex method is shown in Figure A2. The search process terminates when the step size reaches

$$\left| \frac{\Phi^{n+1}(\boldsymbol{p}_1) - \Phi^n(\boldsymbol{p}_1)}{\Phi^n(\boldsymbol{p}_1)} \right| \leqslant 1 \times 10^{-7} \tag{A5}$$

or when the number of iterations reaches 1000. The movement of simplex is shown for the case with $s/h = 1.75$ and $2a/h = 3.50$ in Figure A3. Here the initial simplex and the converged location are highlighted. Note, the movement of simplex is shown only for one initial location for clarity although many more cases with different initial estimates were carried out in the present procedure.